Electronic structure of the nitrogen-vacancy center in diamond from first-principles theory

J. A. Larsson[1] and P. Delaney[1,2]
[1]*Tyndall National Institute, University College Cork, Lee Maltings, Prospect Row, Cork, Ireland*
[2]*School of Mathematics and Physics, Queen's University Belfast, Northern Ireland BT7 1NN, United Kingdom*
(Received 31 July 2007; revised manuscript received 11 February 2008; published 2 April 2008)

The nitrogen-vacancy (NV) center is a paramagnetic defect in diamond with applications as a qubit. Here, we investigate its electronic structure by using *ab initio* density functional theory for five different NV center models of two different cluster sizes. We describe the symmetry and energetics of the low-lying states and compare the optical frequencies obtained to experimental results. We compute the major transition of the negatively charged NV centers to within 25–100 meV accuracy and find that it is energetically favorable for substitutional nitrogens to donate an electron to NV^0. The excited state of the major transition and the NV^0 state with a neutral donor nitrogen are found to be close in energy.

DOI: 10.1103/PhysRevB.77.165201 PACS number(s): 78.20.−e, 78.20.Bh, 78.66.Db, 78.67.Bf

I. INTRODUCTION

The nitrogen-vacancy or NV center is a color center in diamonds containing atomic nitrogen,[1] in which the nitrogen and the vacancy are situated on neighboring lattice positions [see Fig. 1(a)]; the defect can be formed by electron irradiation (to create the vacancies) and subsequent annealing (to allow the vacancy to move toward the nitrogen). The defect has C_{3v} symmetry, with the nitrogen and the vacancy lying on the C_3 axis. It has been well characterized experimentally: usually, it is singly negatively charged, has a paramagnetic ground state ($S=1$) with spatial symmetry A_2, and has a strong dipole allowed $^3A_2 \rightarrow {}^3E$ transition at 1.945 eV.[2] Recently, the NV center has been used as a qubit, and quantum NOT and controlled rotation (CROT) gates have been demonstrated[3] as well as an optical readout of the electronic spin state.[4] The NV center has also been used as a single photon source.[5,6] Creating NV centers in nanodiamonds could open up the possibility of placing NV centers in an array as qubits in a quantum computer. These possible technological uses of the NV center serve as a motivation for our quantitative study of its low-energy electronic structure.[7–12] In this work, we present transition energies calculated from first-principles density functional theory (DFT) of the NV center incorporated into two hydrogen-terminated nanodiamonds with approximate diameters of 1.5 and 1.2 nm [see Fig. 1(b)].

II. THEORY

The NV center can be observed in both neutral NV^0 and charged NV^- states. To describe these states, we first enumerate the relevant single-particle orbitals and then we construct many-body wave functions by differently populating them with electrons.

Earlier works[13–16] described the atomic origin of the NV-center defect wave functions, and we will use their nomenclature to enumerate the molecular orbitals in our clusters. Following Lenef and Rand,[13] there are four sp^3 orbitals pointing into the vacancy, three on the carbons a, b, and c and one orbital d on the nitrogen.

Linear combinations are taken to arrive at the following orthonormal orbitals, which irreducibly transform according to the symmetry group C_{3v}:

$$v = (a + b + c)/\sqrt{3 + 6S}, \tag{1}$$

$$u = (d - \lambda v)/\sqrt{1 - \lambda^2}, \tag{2}$$

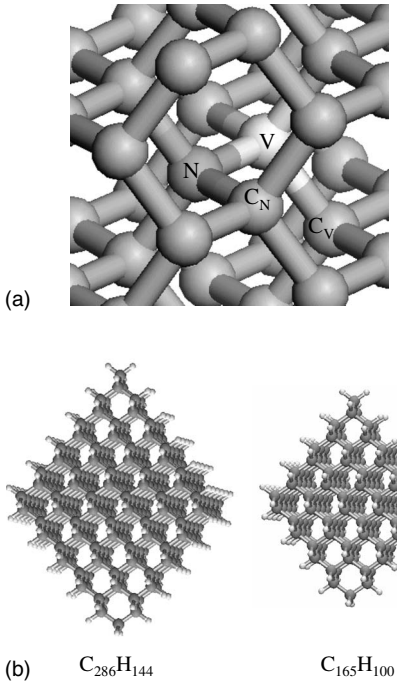

FIG. 1. (a) The NV center in diamond, with obscuring carbons removed for the sake of clarity. C_N denotes carbons that are bonded to the NV center nitrogen, and C_V denotes carbons that are nearest neighbors to the vacancy. (b) Depicted are the hydrogen-terminated diamond nanoclusters $C_{286}H_{144}$ and $C_{165}H_{100}$, of which NV models are based on. They are both T_d symmetric and constitute a triangular-based bipyramid with the base and sides (measured from apex carbon to apex carbon) of each pyramid being 12.70 and 10.16 Å, respectively. This gives a top-to-top distance of 17.96 Å for the large cluster and 14.50 Å for the small cluster.

$$e_X = (2c - a - b)/\sqrt{6 + 6S}, \tag{3}$$

$$e_Y = (a - b)/\sqrt{2 - 2S}. \tag{4}$$

Here, $S=\langle a|b\rangle$ and $\lambda=\langle d|v\rangle$ are overlap integrals. The combination $a+b+c$ and the orbital d are both totally symmetric (a_1 symmetry) and have nonzero overlap and when orthogonalized, give the a_1 states u and v, while the remaining two states form a pair e_X, e_Y of e symmetry. In our DFT calculations, these orbitals mix with all others of like symmetry in a self-consistent cycle; from now on, we use u, v, e_X, e_Y to denote the resulting molecular orbitals. The u orbital that is mostly localized on the nitrogen has the lowest energy, followed by v; the e level is the highest occupied molecular orbital (HOMO). In an infinite crystal, these three energy levels lie in the diamond band gap. In our finite cluster models, we are also interested in the molecular orbital immediately above these, i.e., the lowest unoccupied molecular orbital (LUMO), which has symmetry a_1. We study the NV center by using both models with an added electron and models with a donor nitrogen substituted for a carbon (to get the correct charge state of NV^-, see below), and this LUMO state will have different origins for these two different NV center model types: we denote the respective states by w_- and w_N and by w when we refer to both. We find that these states are not localized around the NV center: w_- is spread over the nanocrystal on the opposite side of the nitrogen from the vacancy, while w_N is centered on the donor nitrogen.

In a neutral NV center (NV^0), there are three carbon and two nitrogen sp^3-hybrid electrons pointing toward the vacancy, resulting in a ground state configuration $u^2v^2e^1$, a doublet, which would Jahn–Teller distort to C_s symmetry. For the NV-center charge state that is of interest to us, the center accepts one electron to become anionic (NV^-), which has a ground state configuration of $u^2v^2e^2$. Besides this configuration, there are two other NV-center excited state configurations relevant to the low-energy electron structure. One configuration of the defect occurs when one electron is excited from v to e, giving $u^2v^1e^3$. There is also an excited configuration $u^2v^2e^1w^1$, in which an electron is excited from the half-filled HOMO e level to the LUMO a_1 state. In the remainder of this section, we will enumerate the various many-body states that can be formed from each configuration.[13–17] A key concern for *ab initio* wave function calculations will be the minimum number of Slater determinants necessary to describe each state.

A. Configuration $u^2v^2e^2$

From four spin orbitals $e_X\uparrow, e_X\downarrow, e_Y\uparrow, e_Y\downarrow$ and two electrons, we could construct $6=\binom{4}{2}$ orthogonal Slater determinants belonging to this configuration. As some of these determinants do not have well-defined space and spin symmetry, we will now construct a better basis by using spatial states with clear symmetry.

To deduce the forms of the spatial wave functions, a matrix representation of C_{3v} for generating elements σ_v and C_3 is taken,

$$\sigma_v = \begin{pmatrix} 1 & 0 \\ 0 & -1 \end{pmatrix}, \quad C_3 = \begin{pmatrix} -1/2 & -\sqrt{3}/2 \\ \sqrt{3}/2 & -1/2 \end{pmatrix}.$$

Lenef and Rand[13] used the transpose of the matrix for C_3, but all the wave function expressions that follow are equally valid for both representations.

By focusing on the two open-shell electrons, the tensor product $e \otimes e$ can be decomposed as $e \otimes e = A_1 \oplus A_2 \oplus E$, showing that the four linearly independent two-electron spatial wave functions have the full range A_1, A_2, E of three spatial symmetries, where the upper case is used for symmetries of many-electron wave functions. There is one spatial wave function of symmetry A_2:

$$\Phi_{A_2} = \tfrac{1}{\sqrt{2}}[e_x e_y - e_y e_x],$$

one of symmetry A_1:

$$\Phi_{A_1} = \tfrac{1}{\sqrt{2}}[e_x e_x + e_y e_y],$$

and a pair of E symmetry:

$$\Phi_E^x = \tfrac{1}{\sqrt{2}}[e_x e_y + e_y e_x],$$

$$\Phi_E^y = \tfrac{1}{\sqrt{2}}[e_x e_x - e_y e_y].$$

The spatial wave function $\Phi_{A_2} = \frac{1}{\sqrt{2}}[e_X e_Y - e_Y e_X]$ is particularly simple. It happens to be independent of the matrix representation chosen, is clearly *antisymmetric* under particle interchange, and so can be multiplied by any of the three triplet spin wave functions $\uparrow\uparrow, \frac{1}{\sqrt{2}}[\uparrow\downarrow + \downarrow\uparrow], \downarrow\downarrow$ to give three states of symmetry $^3A_2$. These are degenerate in the absence of spin-orbit and spin-spin effects. The states with $m_S=+1,-1$ can be written as one Slater determinant. For example, when $\uparrow\uparrow$ is chosen for the spin wave function and all the other electrons in the cluster model are included, we find that the $m_S=+1$ state is

$$^3A_2, \ m_S = +1: \quad |\Psi_{CS} u\uparrow u\downarrow v\uparrow v\downarrow e_X\uparrow e_Y\uparrow\rangle = |\Psi_{CSuv} e_X\uparrow e_Y\uparrow\rangle,$$

where $|\Psi_1, \Psi_2, \ldots, \Psi_N\rangle$ denotes the Slater determinant of the spin orbitals $\Psi_1, \Psi_2, \ldots, \Psi_N$. Here, Ψ_{CS} is the Hartree product of the closed-shell (CS) nanocrystal orbitals; Ψ_{CSu} and Ψ_{CSuv} additionally include the respective doubly filled defect orbitals.

It is this triplet $^3A_2$ state that has been experimentally identified as the ground state. As a paramagnetic ground state, it is unusual and useful: for qubit applications, the spin degeneracy gives us three states to compute with and, as it is the lowest energy level, energy relaxation times out of it will not limit the spin coherence. In reality, due to dipole-dipole interactions between the two electrons, the threefold spin degeneracy is broken and energy relaxation between these three levels occurs, although it is slow. The $m_S=\pm 1$ states remain degenerate due to C_{3v} symmetry but are separated from the $m_S=0$ level by about 2.9 GHz. Long decoherence times are measured: $T_2=0.35$ ms at 300 K.[18]

Qubits tend to be difficult to read out—they have to be decoupled from the environment to achieve long decoherence times, but the same isolation leads to very small signals. In the case of the NV center, optical fluorescence provides a

readout mechanism as at low temperatures it occurs only from the $m_S=0$ level, so if fluorescence is detected, the wave function is projected into this level. Similarly, the lack of detection of fluorescence (a null measurement) causes the density matrix to exponentially collapse into the other levels.

To improve the efficiency of spin readout, it is desirable to know more about the excited E states, the qubit cycles into under laser illumination, and also to know the location and character of any other nearby states as, if these are metastable and dark, they may trap the system and alter the fluorescence yield.

The other three spatial wave functions we can build from the same $u^2v^2e^2$ configuration

$$\Phi_{A_1} = \tfrac{1}{\sqrt{2}}[e_X e_X + e_Y e_Y],$$

$$\Phi_E^X = \tfrac{1}{\sqrt{2}}[e_X e_Y + e_Y e_X],$$

$$\Phi_E^Y = \tfrac{1}{\sqrt{2}}[e_X e_X - e_Y e_Y],$$

depend on the matrices chosen, but the clear *symmetry* of all three wave functions under particle interchange does not. Combining these spatial states with the antisymmetric spin wave function $\frac{1}{\sqrt{2}}[\uparrow\downarrow-\downarrow\uparrow]$ therefore yields three two-electron wave functions, which are antisymmetric under particle exchange and of combined space and spin symmetry $^1A_1$ or ^1E. By including all the closed-shell electrons, we get the following wave functions:

$$^1A_1: \quad \Psi_{A_1} = |\Psi_{\mathrm{CS}uv} e_X\uparrow e_X\downarrow\rangle + |\Psi_{\mathrm{CS}uv} e_Y\uparrow e_Y\downarrow\rangle,$$

$$^1E: \quad \Psi_E^X = |\Psi_{\mathrm{CS}uv} e_X\uparrow e_Y\downarrow\rangle - |\Psi_{\mathrm{CS}uv} e_X\downarrow e_Y\uparrow\rangle,$$

$$^1E: \quad \Psi_E^Y = |\Psi_{\mathrm{CS}uv} e_X\uparrow e_X\downarrow\rangle - |\Psi_{\mathrm{CS}uv} e_Y\uparrow e_Y\downarrow\rangle.$$

Unfortunately, these energy levels are difficult to treat computationally. Most electronic structure codes approximate the quantum many-body problem by introducing some single Slater determinant wave function; the Kohn–Sham determinant in DFT is one example. Complications arise when the simplest many-body wave function with the correct spatial and spin symmetries cannot be written in this form. A glance at the $^1A_1$ and ^1E wave functions shows that they are explicitly given as sums of two Slater determinants. These formulas are not yet definitive evidence that a single Slater determinant is impossible as it is sometimes possible to write a sum of Slater determinants as a single Slater determinant with respect to a new set of orbitals. To check this, one can compute the reduced density matrix $\rho(r_1,r_2)$ from a given wave function[19]: with the norm of ρ chosen so that Tr ρ is the number of electrons, it follows that the normalized wave function can be written as a single Slater determinant of normalized spin orbitals if and only if ρ is idempotent.

For the $^1A_1$ state, we find that ρ_{ij} is in a block-diagonal form, with the subblock of ρ_{ij} corresponding to i,j running through the four spin orbitals $\{e_X\uparrow, e_X\downarrow, e_Y\uparrow, e_Y\downarrow\}$ being $\rho_{ij}=1/2\,\delta_{ij}$. This matrix is clearly not idempotent and, therefore, two Slater determinants are always needed.

The subblock of ρ_{ij} for either of the two ^1E wave functions Ψ_E^X and Ψ_E^Y is the same as for the $^1A_1$ state and, again, two determinants are needed for either of these two states. As we desire to calculate the energy, any unitary linear combination of these states could be used instead if it had a single determinant form. By using the reduced density matrix, one finds that this is possible if and only if one uses *complex* molecular orbitals. For example, $\frac{1}{\sqrt{2}}(e_X+ie_Y)$, $\frac{1}{\sqrt{2}}(e_X-ie_Y)$ can be used to span the ^1E subspace with the following complex single Slater determinants:

$$\tfrac{1}{\sqrt{2}} i\Psi_E^X + \tfrac{1}{\sqrt{2}}\Psi_E^Y = \left|\Psi_{\mathrm{CS}uv}\tfrac{1}{\sqrt{2}}(e_X+ie_Y)\uparrow\tfrac{1}{\sqrt{2}}(e_X+ie_Y)\downarrow\right\rangle$$

and

$$-\tfrac{1}{\sqrt{2}} i\Psi_E^X + \tfrac{1}{\sqrt{2}}\Psi_E^Y = \left|\Psi_{\mathrm{CS}uv}\tfrac{1}{\sqrt{2}}(e_X-ie_Y)\uparrow\tfrac{1}{\sqrt{2}}(e_X-ie_Y)\downarrow\right\rangle,$$

but as most electronic structure codes only use real orbitals, this change of basis is not available to us. Therefore, we can expect difficulties in applying standard Hartree–Fock or DFT to these $^1A_1$ and ^1E states: the single determinant computational state will be a mixture of states of these spatial or spin symmetries.

B. Configuration $u^2v^1e^3$

The next configuration of interest occurs when one of the electrons in the v-derived a_1 symmetry molecular orbital is excited to the partly filled e level. Three electrons in the e level act similar to a hole of e symmetry; together with the unpaired a_1 electron from the v level, it is found that many-body states of this configuration must have spatial symmetry $a_1\otimes e=E$. The hole and electron again give triplet and singlet spin possibilities, giving many-body states with ^3E or ^1E total symmetry. The most visible signature of the NV center—the strong zero-phonon line at 637 nm (1.954 eV)—is attributed to the NV center's major electronic transition from the ground $^3A_2$ level to this ^3E defect term.

Fortunately, the $m_S=1,-1$ members of the ^3E triplet state can be described by using one single Slater determinant, e.g.,

$$^3E,\ m_S=+1: \quad \Psi_E^X = |\Psi_{\mathrm{CS}u} v\uparrow e_X\uparrow e_Y\uparrow e_X\downarrow\rangle,$$

$$^3E,\ m_S=+1: \quad \Psi_E^Y = |\Psi_{\mathrm{CS}u} v\uparrow e_X\uparrow e_Y\uparrow e_Y\downarrow\rangle,$$

and similarly for the $m_S=-1$ states. The singlet states can be expressed by using two Slater determinants (corrected from Ref. 13) as follows:

$$^1E: \quad \Psi_E^X = \tfrac{1}{\sqrt{2}}(|\Psi_{\mathrm{CS}u} v\uparrow e_X\downarrow e_Y\uparrow e_Y\downarrow\rangle - |\Psi_{\mathrm{CS}u} v\downarrow e_X\uparrow e_Y\uparrow e_Y\downarrow\rangle),$$

$$^1E: \quad \Psi_E^Y = \tfrac{1}{\sqrt{2}}(|\Psi_{\mathrm{CS}u} v\uparrow e_Y\downarrow e_X\uparrow e_X\downarrow\rangle - |\Psi_{\mathrm{CS}u} v\downarrow e_Y\uparrow e_X\uparrow e_X\downarrow\rangle),$$

so only an estimate of this state can be computationally obtained.

C. Configuration $u^2v^2e^1w^1$

If the lower energy u and v orbitals are left doubly occupied and one of the e electrons is excited to the first unoccupied orbital (w, symmetry a_1), the $u^2v^2e^1w^1$ configuration is

TABLE I. Distances in Å and angles in deg [the nomenclature C_N and C_V are given in Fig. 1(a)]. The first three columns [NV^- (large), NV-N (large), and N-NV (large)] refer to NV center models built from the large $C_{286}H_{144}$ nanodiamond, while the last two [NV^- (small) and N-NV (small)] refer to NV center models built from the $C_{164}H_{100}$ diamond cluster.

Property	NV^- (large)	NV-N (large)	N-NV (large)	NV^- (small)	N-NV (small)
C_N-N	1.478	1.477	1.476	1.476	1.474
C_V-N	2.771	2.766	2.771	2.776	2.776
C_V-C	1.511	1.500	1.511	1.510	1.510
N-N		7.913	6.043		4.448
C_N-N angle[a]	105.1	105.1	104.9	105.1	104.7

[a]Angle to C_3 axis.

obtained, which may be of comparable energy to $u^2v^1e^3$.

As $e \otimes a_1 = E$, there are four linearly independent spatial wave functions of E symmetry: two with the first electron excited, in which we_X and we_Y transform into each other under C_{3v}, and two with the second electron excited, e_Xw and e_Yw. These pairs do not have a definite particle-interchange symmetry, so a change of basis is made.

The pair $\frac{1}{\sqrt{2}}[we_X + e_Xw]$ and $\frac{1}{\sqrt{2}}[we_Y + e_Yw]$ is *symmetric* under particle interchange and transform into each other under C_{3v}; by multiplying by the singlet spin wave function, we find two linearly independent total wave functions of total symmetry ^1E. By including all the other electrons, we find that each wave function is a sum of two Slater determinants. The exact forms are

$$^1E: \quad \Psi_E^X = |\Psi_{CS} u\uparrow u\downarrow v\uparrow v\downarrow w\uparrow e_X\downarrow\rangle - |\Psi_{CS} u\uparrow u\downarrow v\uparrow v\downarrow w\downarrow e_X\uparrow\rangle$$

and

$$^1E: \quad \Psi_E^Y = |\Psi_{CS} u\uparrow u\downarrow v\uparrow v\downarrow w\uparrow e_Y\downarrow\rangle - |\Psi_{CS} u\uparrow u\downarrow v\uparrow v\downarrow w\downarrow e_Y\uparrow\rangle.$$

By using ρ_{ij}, we can verify that neither of these two wave functions nor any normalized linear combination can be written as a single Slater determinant of normalized spin orbitals.

The second pair $\frac{1}{\sqrt{2}}[we_X - e_Xw]$ and $\frac{1}{\sqrt{2}}[we_Y - e_Yw]$ is antisymmetric and also transform into each other under C_{3v}; multiplying by any of the three triplet spin wave functions gives six linearly independent total fermionic wave functions with symmetry ^3E. When multiplied by either the $\uparrow\uparrow$ or $\downarrow\downarrow$ spin wave functions, both members of the pair give single Slater determinants, allowing us to use conventional codes to estimate the energy of the ^3E term of the $u^2v^2e^1w^1$ configuration. As with the other states of E symmetry, to avoid symmetry breaking, we must average the energy of the two Slater determinants before minimizing it by varying the constituent orbitals. If the $1/\sqrt{2}(\uparrow\downarrow + \downarrow\uparrow)$ triplet spin wave function is used and the wave function is multiplied out, one sees that two Slater determinants are formed.

III. METHOD

The NV center models we use can be characterized by three parameters: cluster size, method of charging the NV center, and NV orientation in the large cluster.

We have constructed NV center models of two different cluster sizes by using the two diamond clusters of T_d symmetry shown in Fig. 1(b) ($C_{286}H_{144}$ and $C_{165}H_{100}$), which we call the *large* and *small* clusters, respectively. Nitrogen-vacancy pairs were created at central positions in each of the clusters by selecting two neighboring carbon atoms on a C_3 axis, replacing one with a nitrogen atom and removing the other. This results in C_{3v} symmetric clusters with neutral NV centers (NV^0), as it is not energetically favorable for the centers to accept an electron from the diamond lattice.

To get the desired charge state of the NV center (NV^-), both large and small clusters have been changed in two ways. In one variant, we add an extra electron to the cluster, giving *anionic* $C_{284}NH_{144}^-$ and $C_{163}NH_{100}^-$ models, which will be called NV^- (large) and NV^- (small), respectively. For the other variant, an additional carbon atom, close to the surface of the cluster and also on the C_3 axis, was replaced by nitrogen, giving the *doped* stoichiometries $C_{283}N_2H_{144}$ and $C_{162}N_2H_{100}$.

Finally, in the doped large cluster, we have room to put the NV center in two different orientations with respect to the dopant N, giving two models that will be called NV-N (large) and N-NV (large), reflecting on which side of the color center the dopant N lies. Note that these two models give rise to different N—N distances (7.913 and 6.043 Å, respectively). For the smaller doped cluster, only the N-NV orientation was used with an N—N distance of 4.448 Å, and it will be called N-NV (small).

All model calculations use the optimized DFT ground state geometries with the Becke-Perdew (BP) exchange-correlation functional and the valence double zeta polarized [VDZ(P)] basis set as provided by the TURBOMOLE suite of programs.[20] All models adapt a $^3A_2$ ground state, and vertical transitions have been calculated from these equilibrium structures. The local geometry around the NV center of the clusters is given in Table I. As can be seen from Table I, the five cluster models show remarkable similarities in structure. All of the states have been calculated within the full symmetry of the system by using the ΔSCF method, which was possible because the lowest state in different symmetry groups or distinctly different occupations was computed. Time-dependent DFT would be needed for higher-lying states with the same state symmetry.

The size and stability of the $C_{286}H_{144}$ (large) and $C_{165}H_{100}$ (small) clusters ensure a proper description of stable diamond nanoparticles. The C-C bond lengths in both clusters range from 1.539 to 1.565 Å, wherein the central part of the

TABLE II. Excited state transition energies ΔE are given in eV and the spin contaminations $\langle S^2 \rangle$ are in units of $\hbar^2$. The orbital nomenclature u, v, e, and w is given in Sec. II. $^1E+^1A_1$ denotes a mixture of the two states.

Model system	Property	$u^2v^2e^2$ $^1E+^1A_1$	$u^2v^1e^3$ ^3E	$u^2v^2e^1w^1$ ^3E	$u^2v^2e^1w^1$ ^1E	$u^2v^1e^3$ ^1E
NV^- (large)	ΔE	0.641	1.867	1.878[a]	1.877[a]	2.296
	$\langle S^2 \rangle$	1.000	2.311	2.256	1.256	1.259
NV-N (large)	ΔE	0.648	1.886	1.766[b]	1.765[b]	2.285
	$\langle S^2 \rangle$	1.000	2.280	2.258	1.258	1.254
N-NV (large)	ΔE	0.643	1.912	1.558[b]	1.558[b]	2.366
	$\langle S^2 \rangle$	1.000	2.403	2.257	1.257	1.261
N-NV (small)	ΔE	0.640	1.922	1.343[b]	1.342[b]	2.384
	$\langle S^2 \rangle$	1.000	2.327	2.257	1.258	1.259
NV^- (small)	ΔE	0.644	1.847	1.883[a]	1.888[a]	2.277
	$\langle S^2 \rangle$	1.000	2.311	2.256	1.256	1.254

[a]Transition energy values ΔE that represent excitation charge transfer from the negatively charged NV center to a delocalized conduction-band-like cluster LUMO state (see text).

[b]Transition energy values ΔE that represent excitation charge transfer from the negatively charged NV center to the positively charged dopant N, rather than an excitation within the negatively charged NV center (see text).

cluster has a very uniform distribution of bond lengths (1.557–1.565 Å). These central bond lengths reflect the overestimated bulk bond length acquired at this level of theory. The experimental bond length in bulk diamond is 1.545 Å. For a comparison to the experimental band gap of bulk diamond (5.5 eV), we report both the HOMO-LUMO gap, at 4.68 eV (large) and 4.90 eV (small), and the energy of the first excited state of the cluster, which is computed to be 4.73 eV (large) and 4.95 eV (small) higher in energy than the ground state with the ΔSCF method. The HOMO-LUMO gap and first excited state values of the large nanodiamond cluster are farther from the bulk diamond band gap than the corresponding values for the small cluster. This is due to a well-known nanoparticle size effect; since small particles have less mixing of energy levels, which gives narrower bands or quantized levels, smaller clusters have larger band gaps. The bigger cluster gives values closer to the typically underestimated BP/VDZ(P) bulk limit.

A measured band gap involves an excitation to the conduction band or, alternatively, a relaxation from the conduction band to the valance band, and can only be accounted for by the calculation of an excited state of one form or another. It is therefore quite remarkable that the HOMO-LUMO gap, which can only be used as a rough estimate of the band gap (by using Koopman's theorem), gives a number so close in energy to the calculated excited state transition.

Although the NV center models in this study represent rather small nanoparticles, they do correspond to a reasonable approximation of the NV center in bulk diamond. As compared to a periodic supercell calculation, our cluster models of diamond are rather large. Even though they do incorporate surface effects, this study of the NV center in nanodiamonds is, on the other hand, free from any spurious defect-defect interactions between neighboring cells that are hard to root out when using the supercell approach (see, e.g., Ref. 21).

We have also tried to use restricted open-shell Hartree–Fock to calculate the states of the NV center, but the error without electron correlation is too severe. Thus, we chose not to report these energies. A future study on the position of the individual $^1A_1$ and ^1E states—of which only a mixture can be calculated in this work—by using the Monte Carlo configuration interaction method[22] will be published elsewhere.

IV. RESULTS AND DISCUSSION

The characteristic feature of the NV center is its $^3A_2$ paramagnetic ground state, which arises from placing two electrons in the e-symmetry HOMOs of the cluster ($u^2v^2e^2$). Our calculations show, in accordance with another work,[23] that these HOMOs are centered on the vacancy, i.e., the extra electron, either added to the cluster [NV^- (large) and NV^- (small)] or provided by the additional N [N-NV (large), NV-N (large), and N-NV (small)], is primarily located on the three carbon atoms surrounding the vacancy. However, both the anionic and doped cluster models used in our study describe the negatively charged NV^- state. This means that the N-NV and NV-N models would be better described as N^+-NV^- and NV^--N^+, respectively, and shows that energy minimization causes substitutional nitrogen to act as electron donor to the NV center. It is a rather remarkable result that an additional electron and an additional substitutional N give the same NV^- state after energy and geometry minimizations, and it is manifested in the geometrical parameters and on-center excitation energies of all our models being almost identical (see Tables I and II). This also indicates that for localized NV excitation energies, both cluster sizes are within the bulk limit. This is, however, not true for the electronic transitions between e and w_N, as will be shown below.

The energetics of the low-lying many-body states from DFT are listed in Table II and graphically represented to-

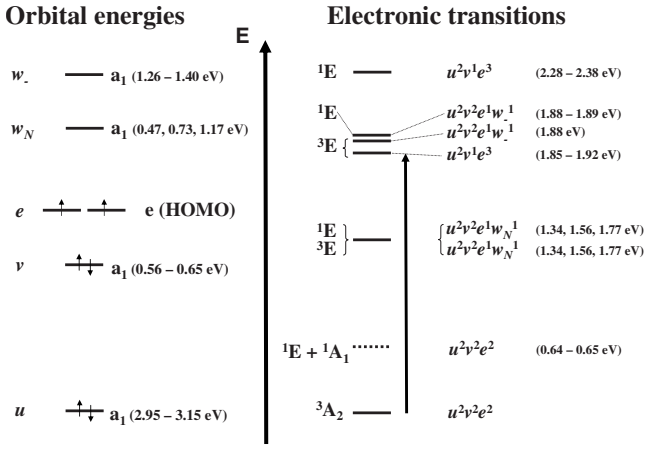

FIG. 2. Left-hand side: The orbital occupation of the NV center ground state. The orbital nomenclature (u, v, e, and w_-, and w_N) is given in Sec. II. The range of orbital energies with respect to the HOMO level (absolute values) is given in parentheses for the different NV center models. Explicit values are given for w_N from the three doped cluster models, since this strongly depends on the distance between the NV center and the donor N. Right-hand side: The electronic transitions of the NV center as calculated with DFT. The transition energies are similarly given as ranges (cf. Table II). Explicit values from the three doped cluster models are given for the e to w_N excitations, since they strongly depend on the distance between the NV center and the donor N.

gether with the single-particle orbitals in Fig. 2. As the characteristic $^3A_2$ ground state ($u^2v^2e^2$) can be modeled with one Slater determinant, we find a correspondingly small spin contamination in our computational wave function of $S^2=2.009\hbar^2$ in all the five NV center models, which compares well to the exact $S^2=s(s+1)\ \hbar^2=2\hbar^2$. We take the energy of this state to be zero.

Another characteristic feature of the NV center in diamond is its major optical transition, whose zero phonon line (ZPL) at 1.945 eV (637 nm) is associated with the ^3E state with a $u^2v^1e^3$ occupation. The best previous calculation of ZPL was by Goss *et al.*,[16] who obtained "fair agreement" with a transition energy of 1.77 eV. Fortunately, as these ^3E states can also be modeled with a single determinant, our computational state has an acceptable spin contamination in all our NV-center models ($S^2=2.256\hbar^2-2.258\hbar^2$) and a vertical excitation energy between 1.847 and 1.922 eV, which compares quite well to the measured ZPL.

There is also a forbidden singlet state of ^1E symmetry with the same $u^2v^1e^3$ configuration. As the ^1E state needs two Slater determinants and our computational state is a single determinant, our result exhibits a significant spin contamination ($S^2=1.254\hbar^2-1.259\hbar^2$), wherein energies around 2.3 eV can only be used as an estimate of the true energy. Nevertheless, as this state seems to have a significantly higher energy, we suggest that it does not play a role in the normal use of the major optical transition of the NV center. We note that the singlet-triplet splitting here is approximately 0.4 eV, whereas for the $u^2v^2e^1w_N^1$ and $u^2v^2e^1w_-^1$ configurations, it is on the order of meV: this is due to the larger exchange integrals between two localized e levels as compared to a localized e level and distant w_N or w_- orbitals.

The remaining dark states—^1E and $^1A_1$ symmetries from the $u^2v^2e^2$ configuration—could interfere with the decay to the ground state. Both are two-determinant wave functions, so the DFT single-determinant wave function we use is a mixture of the two states. Theoretical methods that explicitly account for electron correlation are needed to get the separation between two such states and such methods are too computationally demanding to be feasible for our models. However, we think some useful information might be conveyed by our computations of the mixed state as the excitation energy turns out to have a very low spread of values between the different cluster models.

Regarding the LUMO, the two anionic model variants differ from the three doped NV center models but, as shown above, all of the models in this study have the negatively charged NV^- state as the ground state. In the anionic NV center models [NV^- (large) and NV^- (small)], we will make the working assumption that the LUMO (symmetry a_1) is of conduction band origin as it extends over half of the cluster on the side of the nitrogen opposite to the vacancy. Jones *et al.*[24] found that the V-N_3 defect creates a shallow electron trap below the conduction band that is not derivable from the four sp^3 orbitals surrounding the vacancy, so further analysis is necessary to find the exact nature of this state for the NV center. Summarizing, the excitation to the LUMO of the cluster describes a transition to a conduction-band-like state for the large and small anionic NV^- models.

In the doped cluster models [N-NV (large), NV-N (large), and N-NV (small)], the donor nitrogen has an a_1 state, which becomes the LUMO. In addition, there is hybridization between this donor N state and the a_1 state of conduction band origin. The configuration here is $u^2v^2e^1w_N^1$ and in ^3E or ^1E forms, lies 1.342–1.766 eV above the $^3A_2$ ground state, as can be seen in Table II. These positive numbers give further proof that energy minimization leads to a neutral substitutional nitrogen donating an electron to the NV^0 center, that is, charging the center by going from formally N^0-NV^0 (NV^0-N^0) to N^+-NV^- (NV^--N^+). This represents the natural charge distribution in nitrogen-containing diamond, in which the NV center is usually negatively charged.[25] In some cases, NV^0 is more stable than NV^-, which we attribute to the presence of additional defects that are more stable with an additional electron than the NV center.[26]

Laser light may decharge the NV^- form of the NV center by causing the transition to the ^3E and ^1E excitations with configuration $u^2v^2e^1w_N^1$ in the doped clusters: the extra electron gets transported to a nearby nitrogen donor. We suggest that this could explain why the NV center sometimes becomes dark when pumped with a laser.[26] As dipole matrix elements exponentially decrease with distance, this process should be negligible except for very close nitrogens. For such donors, we find that the excitation energy strongly depends on the N···N distance in the doped clusters, while always being lower in energy than configuration $u^2v^2e^1w_-^1$ excitations for NV^- (large) and NV^- (small). This distance dependence can be understood as mixing with the NV center perturbed a_1 conduction band state. When the NV center and the donor N are sufficiently far apart, there will be less mixing and the localized donor N state will be closer to the conduction band edge.

Collins[25] suggested that electrons in diamond defects are not in thermal equilibrium, so the mechanism for decharging and charging the NV center is of interest. Direct electron tunneling is unlikely to be the mechanism unless the nitrogen to NV center distance is short: the $\langle w_N|H|e_{X,Y}\rangle$ molecular orbital matrix element exponentially drops with distance. Conduction-band-mediated motion does not have this problem, but the Boltzmann factor for excitation from nitrogen impurities is $e^{-1.7(40)}-10^{-30}$ at room temperature.

It has been suggested that positively charged substitutional N atoms that are not identical to the donor N could interfere with the NV center transitions, involving the charging excitation of substitutional N to the conduction band.[23] We want to emphasize that if the diamond is not in thermal equilibrium, then location matters. The NV center is likely to interact only with the nearest nitrogens and mostly so with the donor nitrogen, as in the $u^2v^2e^1w_N^1$ state of our calculations, either by direct hopping for very nearby donors or through a two step process (excitation to the conduction band followed by relaxation).

We also want to point out that in our calculations, these decharged states with configuration $u^2v^2e^1w_N^1$ can be very close in energy below the ^3E $u^2v^1e^3$ excited state of the major transition, especially for NV-N (large), wherein the distance to the donor N is largest. In the experiment, the donor N is even further separated from the NV center and the transitions would be even closer in energy to the major transition. The possibility of a two step process through the conduction band and the closeness in energy of the $u^2v^2e^1w_N^1$ and ^3E $u^2v^1e^3$ states might make the process more probable. For example, in the NV-N (large) cluster, the ^3E $u^2v^2e^1w_N^1$ decharged state lies 0.12 eV below the ^3E $u^2v^1e^3$ excited state of the major optical transition of the NV center, and this energy difference could be supplied or absorbed by diamond phonons. When illumination causes the NV^- form of the NV center to cycle between the $^3A_2$ and ^3E states, occasionally, the ^3E $u^2v^1e^3$ state may decharge in this way to a nearby nitrogen (^3E or ^1E $u^2v^2e^1w_N^1$). This could explain the frequent transitions between NV^0 and NV^- that were observed in a single center by Gaebel *et al.*[26] Additionally, laser light in near resonance with the major transition will be in near resonance with this charging/decharging transition and could make it a by-product for very nearby donors.

When NV centers are decharged by laser pulses, the electron has been observed to return with a range of rates, and some centers that quickly decharge charge again only slowly. It has been suggested that the ionization of nitrogens can move around between donors because if this happens while the center is decharged, an increased donor-NV distance would explain the slower rate of return. If this process also occurs during the cycling between the $^3A_2$ $u^2v^2e^2$ and ^3E $u^2v^1e^3$ states upon steady illumination, the resulting occasional change in the identity of the donor nitrogen and the local electrostatic environment may explain the observed jitter in the ZPL, while if only one nitrogen donor is nearby, the ZPL should be stable.[27] Ionization tunneling directly between several nearby nitrogens may also be a source of jitter.

The close agreement of the excited state transitions between the models, together with the nearly identical geometrical parameters, is a testament that one of the models is as sound as the other. In effect, the N-NV (large), NV-N (large), and N-NV (small) models validate that the large and small NV^- models are properly handled by using standard DFT in conjunction with a standard quality basis set. It is, of course, the extended size of the cluster, which completely houses the additional electron, which makes the use of diffuse functions redundant. It is only when anionic electrons reside on or near the surface of a molecule or cluster that additional low exponent basis functions are needed because they describe the part of space where the electron density is substantial for anions but not for neutral species.

V. CONCLUSIONS

First-principles DFT simulations have been used to provide insights into the excited electronic states of the NV center in diamond. To this purpose, we have identified which states can be modeled with one Slater determinant. Good agreement has been found between our different models. We have found good agreement with experiment on the major electronic transition of the center, $^3A_2$ of $u^2v^2e^2$ to ^3E of $u^2v^1e^3$: our vertical excitations are in the range of 1.847–1.922 eV and the experimental ZPL is 1.945 eV. We have computational evidence suggesting that the ^1E state of this latter configuration lies a further $\sim$0.4 eV higher in energy.

By finding that the $u^2v^2e^1w_N^1$ configuration in doped clusters lies above the $^3A_2$ state of the $u^2v^2e^2$ configuration, we have shown that energy minimization causes nearby nitrogen atoms to act as donors to the NV center and we have speculated on the mechanisms that allow this charging/decharging transition. We speculate that this transition could be experimentally seen. Its energy significantly depends on the distance to the donor nitrogen and may depend on cluster size, allowing diamond phonons to assist the transition for larger distances. As it is of different character than on-center excited states, direct hopping transition matrix elements should exponentially decay with distance. Slightly higher energies have been found for a decharging transition to the conduction band.

The excited states needing two or more Slater determinants could only be approximately dealt with in standard DFT and possessed significant spin contamination. Multideterminant calculations that use correlated methods are necessary to accurately find these states. However, it seems that there are two low-lying singlet states that could act as dark states and trap the center.

ACKNOWLEDGMENTS

We acknowledge funding support from Science Foundation Ireland and from the European Union project Nanocage. J.A.L. thanks the Nationellt Superdator Centrum (NSC, Sweden) for the generous allotment of computer time.

[1] A. Beveratos, R. Brouri, T. Gacoin, J.-P. Poizat, and P. Grangier, Phys. Rev. A **64**, 061802(R) (2001).
[2] A. Uedono, K. Mori, N. Morishita, H. Itoh, S. Tanigawa, S. Fujii, and S. Shikata, J. Phys.: Condens. Matter **11**, 4925 (1999).
[3] F. Jelezko, T. Gaebel, I. Popa, M. Domhan, A. Gruber, and J. Wrachtrup, Phys. Rev. Lett. **93**, 130501 (2004).
[4] F. Jelezko, T. Gaebel, I. Popa, A. Gruber, and J. Wrachtrup, Phys. Rev. Lett. **92**, 076401 (2004).
[5] R. Brouri, A. Beveratos, J.-P. Poizat, and P. Grangier, Opt. Lett. **25**, 1294 (2000).
[6] C. Kurtsiefer, S. Mayer, P. Zarda, and H. Weinfurter, Phys. Rev. Lett. **85**, 290 (2000).
[7] C. Santori, P. Tamarat, P. Neumann, J. Wrachtrup, D. Fattal, R. G. Beausoleil, J. Rabeau, P. Olivero, A. D. Greentree, S. Prawer, F. Jelezko, and P. Hemmer, Phys. Rev. Lett. **97**, 247401 (2006).
[8] K. Ishioka, M. Hase, M. Kitajima, and H. Petek, Appl. Phys. Lett. **89**, 231916 (2006).
[9] L. Childress, M. V. G. Dutt, J. M. Taylor, A. S. Zibrov, F. Jelezko, J. Wrachtrup, P. R. Hemmer, and M. D. Lukin, Science **314**, 281 (2006).
[10] R. Hanson, O. Gywat, and D. D. Awschalom, Phys. Rev. B **74**, 161203(R) (2006).
[11] R. Hanson, F. M. Mendoza, R. J. Epstein, and D. D. Awschalom, Phys. Rev. Lett. **97**, 087601 (2006).
[12] J. J. L. Morton, Nat. Phys. **2**, 365 (2006).
[13] A. Lenef and S. C. Rand, Phys. Rev. B **53**, 13441 (1996).
[14] J. P. Goss, R. Jones, P. R. Briddon, G. Davies, A. T. Collins, A. Mainwood, J. A. van Wyk, J. M. Baker, M. E. Newton, A. M. Stoneham, and S. C. Lawson, Phys. Rev. B **56**, 16031 (1997).
[15] A. Lenef and S. C. Rand, Phys. Rev. B **56**, 16033 (1997).
[16] J. P. Goss, R. Jones, S. J. Breuer, P. R. Briddon, and S. Öberg, Phys. Rev. Lett. **77**, 3041 (1996).
[17] N. B. Manson, J. P. Harrison, and M. J. Sellars, Phys. Rev. B **74**, 104303 (2006).
[18] T. Gaebel, M. Domhan, I. Popa, C. Wittmann, P. Neumann, F. Jelezko, J. R. Rabeau, N. Stavrias, A. D. Greentree, S. Prawer, J. Meijer, J. Twamley, P. R. Hemmer, and J. Wrachtrup, Nat. Phys. **2**, 408 (2006).
[19] P. Delaney and J. C. Greer, Comput. Mater. Sci. **28**, 240 (2003).
[20] R. Ahlrichs, M. Bär, M. Häser, H. Horn, and C. Kölmel, Chem. Phys. Lett. **162**, 165 (1989).
[21] A. Höglund, C. W. M. Castleton, and S. Mirbt, Phys. Rev. B **72**, 195213 (2005).
[22] J. C. Greer, J. Comput. Phys. **146**, 181 (1998).
[23] P. Tamarat, T. Gaebel, J. R. Rabeau, M. Khan, A. D. Greentree, H. Wilson, L. C. L. Hollenberg, S. Prawer, P. Hemmer, F. Jelezko, and J. Wrachtrup, Phys. Rev. Lett. **97**, 083002 (2006).
[24] R. Jones, J. P. Goss, P. R. Briddon, and S. Öberg, Phys. Rev. B **56**, R1654 (1997).
[25] A. T. Collins, J. Phys.: Condens. Matter **14**, 3743 (2002).
[26] T. Gaebel, M. Domhan, C. Wittmann, I. Popa, F. Jelezko, J. Rabeau, A. Greentree, S. Prawer, E. Trajkov, P. R. Hemmer, and J. Wrachtrup, Appl. Phys. B **82**, 243 (2006).
[27] N. B. Manson (private communication).